Raytheon
BBN Technologies

UNIVERSITY OF MICHIGAN

Space Debris Elimination (SpaDE) Phase I Final Report

NASA NIAC -- 11- 11NIAC-0241

Daniel Gregory

JF Mergen

Aaron Ridley

12 Dec 2012

The material is based upon work supported by NASA under award 11-11NIAC-0241.

Any opinions, findings, and conclusions or recommendations expressed in this material are those of the author(s) and do not necessarily reflect the views of the National Aeronautics and Space Administration.

Raytheon
BBN Technologies

Table of Contents

1 Executive Summary

SpaDE phase I has evaluated the viability of the SpaDE concept and shown that space debris can be mitigated in lower LEO orbits using gravity wave perturbations from relatively low altitudes.

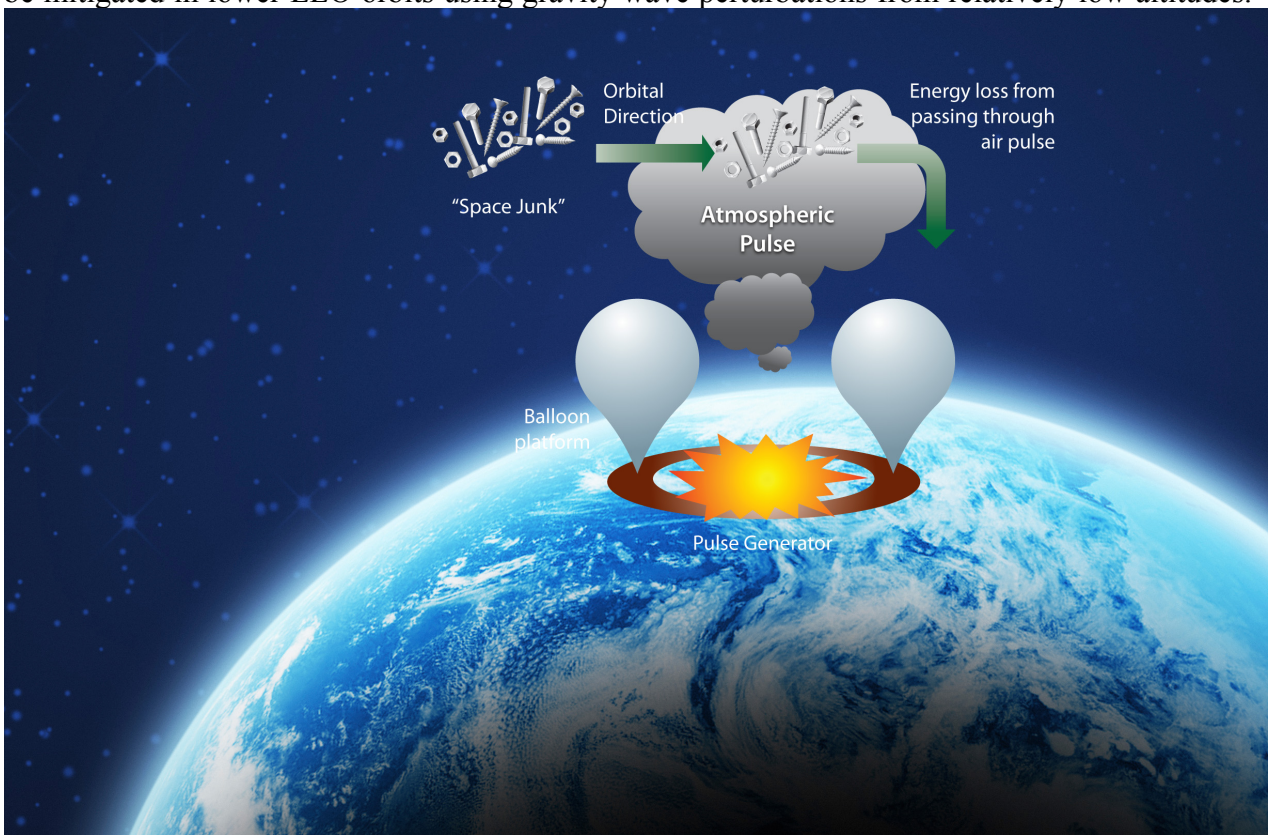

2 Introduction

The amount of debris in low Earth orbit (LEO) has increased rapidly over the last twenty years, threatening vital satellites. The prevalence of space debris increases the likelihood of cascading collisions, creating debris belts that render many orbits effectively unusable. This cascading effect, in which debris generation outstrips debris re-entry, is known as Kessler Syndrome and some models indicate that it is happening now.

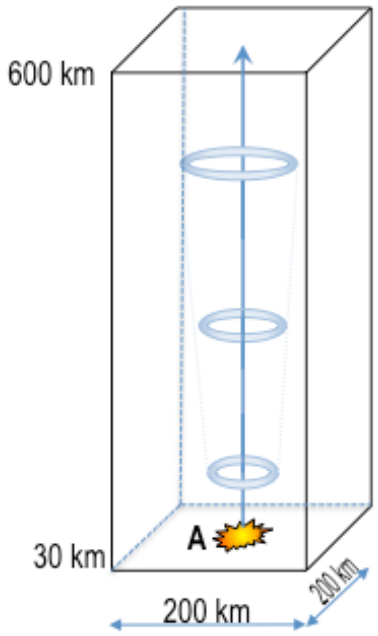

Figure 1: SpaDE launches air pulses from point A into LEO

The Space Debris Elimination (SpaDE) project is investigating the use of focused pulses of atmospheric gases to accelerate the rate of decay on debris by creating a temporary drag that causes the debris to reenter the atmosphere sooner than would naturally occur. The pulses themselves soon fall back into the atmosphere, leaving no residual trace in orbit to interfere with LEO satellites. Air pulse braking can be effective on debris ranging in size from paint flakes to spent booster casings.

In contrast to other proposed methods, SpaDE is failsafe in that it places no device (e.g., a net) in orbit where a malfunction would create new debris. SpaDE should provide a lower cost alternative to orbiting a removal system. The use of a pulse will enable SpaDE to cover a debris field resulting from a particular event, such as the Chinese destruction of a weather satellite in 2007, or the 2009 Iridium satellite collision (figure 2). The SpaDE system window of opportunity is measured in 10s of seconds and kilometers, meaning there is a wide range of possible starting conditions that will yield favorable results.

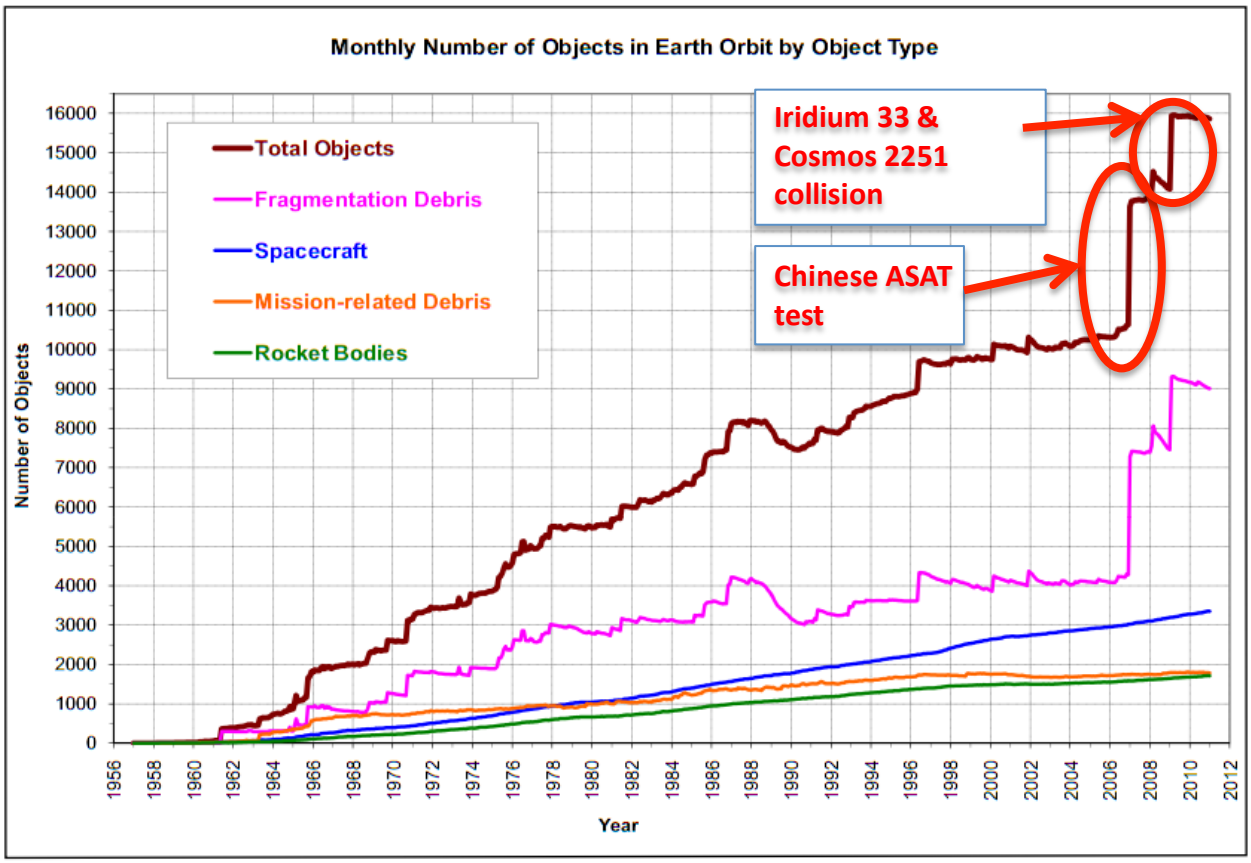

Figure 2: Satellites Around Earth -- Figure courtesy of NASA and the Orbital Debris Program Office

SpaDE will use a device mounted on an airborne platform (e.g., a high-altitude balloon) to propel pulses of atmospheric air into space. The operational altitude of the platform would be between 25 and 35km, to minimize drag effects from the dense lower atmosphere.

SpaDE will generate air pulses that maintain their cohesion during transit to orbital altitudes. In Phase 1 we explored gravity waves to produce pulses that remain coherent and analytically validated the physics underpinning the SpaDE concept.

3 Concept Explanation

For SpaDE Phase 1, we concentrated on developing a model that could test a variety of perturbation modalities. This effort started with the University of Michigan's Global Ionosphere-Thermosphere Model (GITM) changes. The secondary efforts focused on the debris behavior moving through the perturbation.

Perturbation Modalities describe how atmospheric perturbations, such as vortices, shaped-charge-induced gravity waves, and laminar flows propagate from the perturbation generator to the altitude of the space debris. Studying these perturbations will allow the SpaDE system to be designed for maximum performance or economy.

We addressed the major feasibility issues of perturbation in Phase 1, with a focus on simple gravity-wave perturbations. The major focus was to modify the model to analyze gravity wave perturbations from lower altitudes in a small region of the atmosphere.

Debris Behavior in Phase I focused on modeling the interactions of the perturbed atmosphere with the space debris target. Debris behavior looks at the impact the perturbation has on the debris. In this study we calculate the deltaV of the debris as it interacts with the perturbation. We also look at the timing of the perturbation and the debris. One of the major problems with debris removal is that the timing is critical to many solutions. We show that SpaDE does not have tight timing requirements. We measure our window of opportunity in 10s of seconds instead of nanoseconds. The effectiveness of the system is also dependent on the position of the debris to the perturbation. Many pieces of debris do not have a pinpoint location and the uncertainty error, as a function of the distance to the projected ephemeris is measured in kilometers. So a system that has an effective range of a kilometer across might not hit the targeted debris at all. This is one of the main issues with the laser based systems, they need pinpoint accuracy of the target that they are trying to hit. SpaDE does not have this constraint. SpaDE tolerates approximate debris position data.

Our model is based on several simplifying assumptions. We fix the altitude of the debris as it traverses the perturbation area, whereas in reality, as the debris is affected by the perturbation, its altitude will drop. Also, our model freezes the perturbation while calculating the drag effects on the debris. In reality, the perturbation will be changing while the debris is traversing. The effects of these assumptions should not significantly impact the accuracy of our findings.

GITM is a 3-dimensional spherical code that models the Earth's thermosphere and iono- sphere system using a stretched grid in latitude and altitude Ridley et al. [2006]; Deng et al. [2008a,b]; Pawlowski and Ridley [2008, 2010]. GITM explicitly solves for the neutral densities of O(3P),O(1D), O2, N(2D), N(4S), N2, and NO (instead of mass mixing ratios), densities of the

ion species O+(4S), O+(2D), O+(2P), O2+, N+, N2+, and NO+, 3-dimensional neutral and ion velocities, and neutral, ion, and electron temperatures.

The model is fully parallel using a block-based two-dimensional domain decomposition in the horizontal coordinates [Oehmke and Stout, 2001; Oehmke, 2004]. The number of latitude and longitude blocks can be specified at runtime, so the horizontal resolution is extremely flexible. One of the major differences between GITM and other models of the upper atmosphere is that altitude is used as the vertical coordinate as opposed to pressure. The altitude spacing is set at approximately 1/3 of the neutral scale height, and setting the lower boundary and the number of grid points specifies the vertical domain.

3.1 Non-hydrostatic Processes

GITM is the only coupled ionosphere-thermosphere model to relax the hydrostatic assumption. In other words, GITM self-consistently solves the momentum equation in the vertical direction. There are a number of positive consequences of this, as well as a few negative ones. For one, GITM is capable of modeling sound waves in the vertical direction [Deng et al., 2008a]. However, because of their fast propagation, the advective time-step is limited to about 2-3 seconds. Such a small time step allows the model to capture physics that other GCMs may miss, such as chemical reactions, but at a cost: the simulations take longer to run. On the other hand, GITM can accurately model the strong vertical winds in the auroral zone due to heating caused by ion variability [Yiğit and Ridley, 2011; Yiğit et al., 2012]. Relaxing the hydrostatic assumption also allows for the use of non-constant gravity throughout the vertical domain, which Deng et al. [2008b] showed has a significant effect on the model solution.

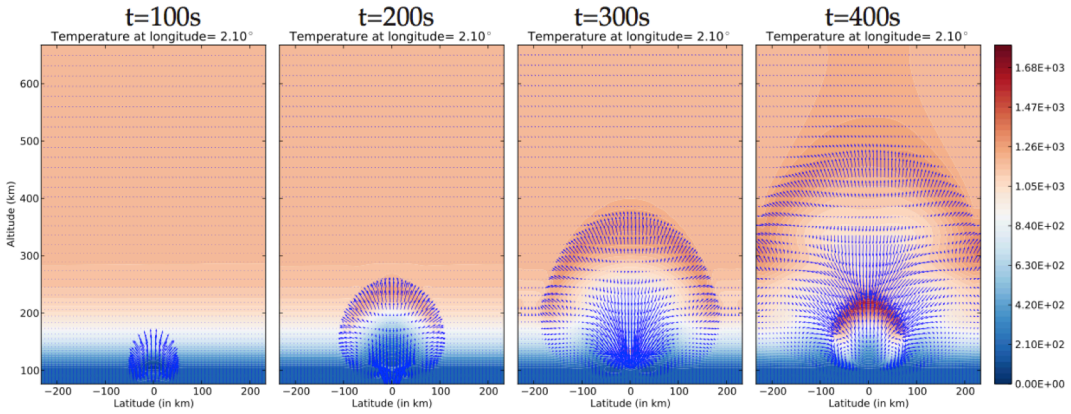

Figure 3: GITM Simulation results of the thermospheric response to a 20km×20km energy input.

Figure 3 shows a recent simulation of a large temperature increase at 80km altitude within a limited-region version of GITM. The horizontal resolution in this case was about 5km×5km. A mushroom cloud type of formation was observed, with a shock structure that led the perturbation along with a secondary perturbation that propagated slower than the speed of sound.

3.2 Model Drivers

GITM is capable of being driven by several different descriptions of the solar flux. For idealized studies, or to compare to other models, such as MSIS or IRI, GITM can be driven by the F10.7 flux [e.g., Hinteregger et al., 1981; Richards et al., 1994; Tobiska, 1996; Woods and Rottman, 2002]. During time periods when data is available, GITM can use observations from the Solar EUV Experiment (SEE) on board the Thermosphere Ionosphere Mesosphere Energetics and Dynamics (TIMED) satellite [Woods et al., 2005, 2008]. In addition, results from the Flare Irradiance Spectral Model (FISM), which specifies the solar EUV irradiance on a 1-minute time scale at 1-nm spectral resolution, and therefore includes estimations of irradiance increases due to solar flares [Chamberlin et al., 2007] can be used to drive the model. In all of the above cases, the solar flux is binned into 59 wavelengths that are commonly used to describe the ionization and heating in the thermosphere [Torr et al., 1979; Solomon et al., 1988; Woods and Rottman, 2002].

GITM is also coupled to several models of the high-latitude ionospheric electrodynamics. For example, GITM can be run using results from the assimilative mapping of ionospheric electrodynamics (AMIE) technique [Richmond and Kamide, 1988; Richmond, 1992]. Also, the Weimer [1996], Foster et al. [1983], Heppner and Maynard [1987], or Ridley et al. [2000] electrodynamic potential patterns can be used to drive the high-latitude ionospheric circulation, and the auroral dynamics can be specified using the Hardy et al. [1987]; Fuller-Rowell and Evans [1987] or Newell et al. [2009] particle precipitation patterns.

3.3 Model Validation

Figure 4 shows a comparison between orbit averaged CHAMP mass density measurements and GITM results for the May 14-15, 2005 storm. In this case, GITM was driven using FISM measurements to specify the solar flux and Weimer [2005] with Fuller-Rowell and Evans [1987] to specify the high-latitude dynamics. The right plots show comparisons between GITM (top right) and the global network of total electron content (TEC) measurements (top left) for a specific time just before the storm period. The bottom plots show the absolute (left) and relative (right) differences.

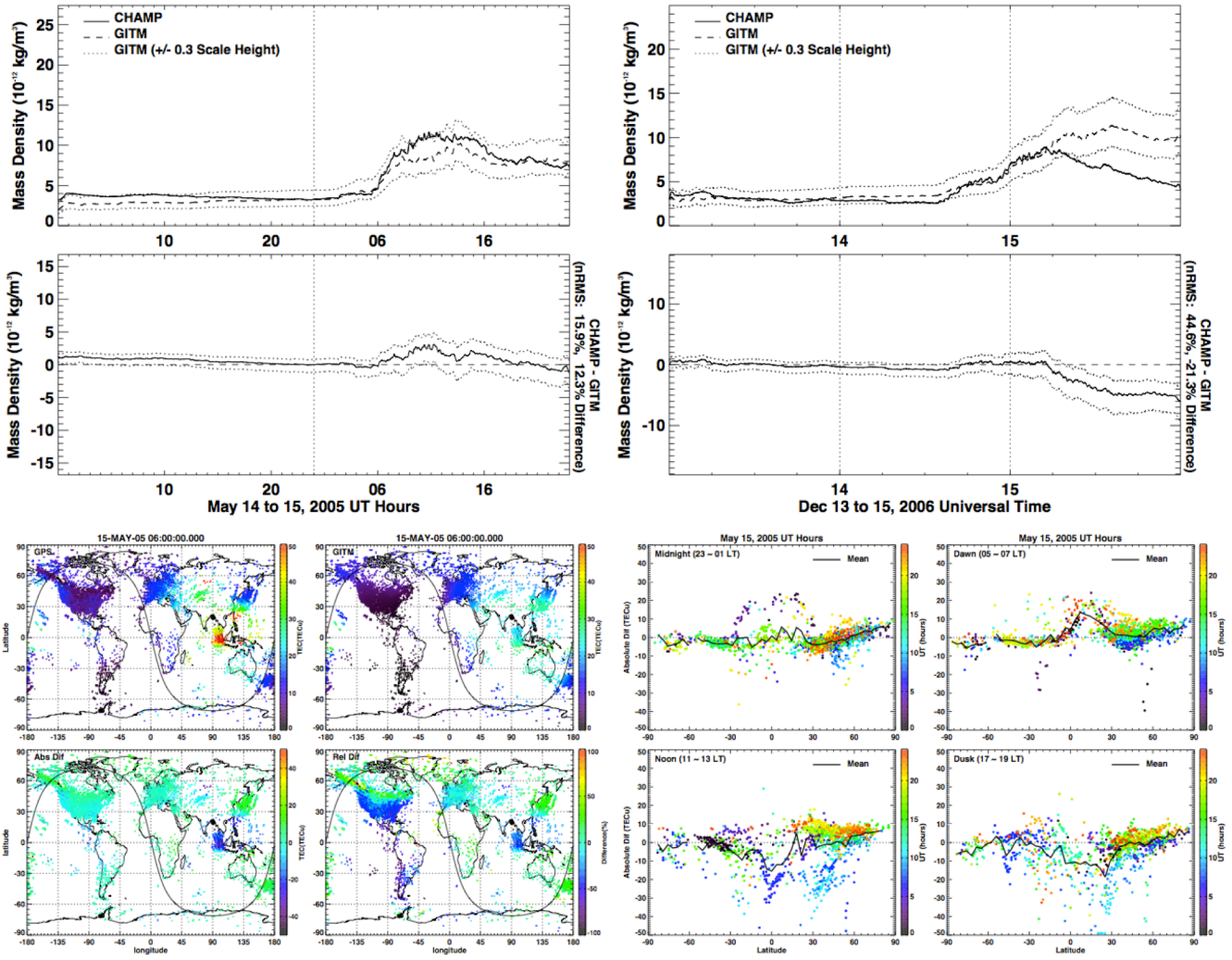

Figure 4: GITM comparisons to various data sources, including CHAMP (top plots) and global TEC (bottom plots).

4 Pulse Generation

The SpaDE Phase 1 project has produced analytic results validating the approach. We adapted the University of Michigan's Global Ionosphere-Thermosphere Model (GITM) to model a rectangular column of atmosphere extending from 80 to 600km in altitude and having a square cross sectional size of 200km by 200km. To understand the bounds of the problem, we looked at the what forces would be required to bring a typical piece of debris down in a single revolution. This required us to try and achieve a 2000% change in ρ over roughly a 200km stretch in the debris path. The model indicates that an explosive pulse of tractable size would produce a 200km diameter disc parallel to the surface of the earth 400km in height, and with a pressure differential over 2000% of ρ, as shown in Figure 3 below. A piece of debris with a coefficient of drag of 1.6

or greater traversing the diameter of this disk would have its trajectory rapidly degraded, potentially inducing re-entry within one orbit.

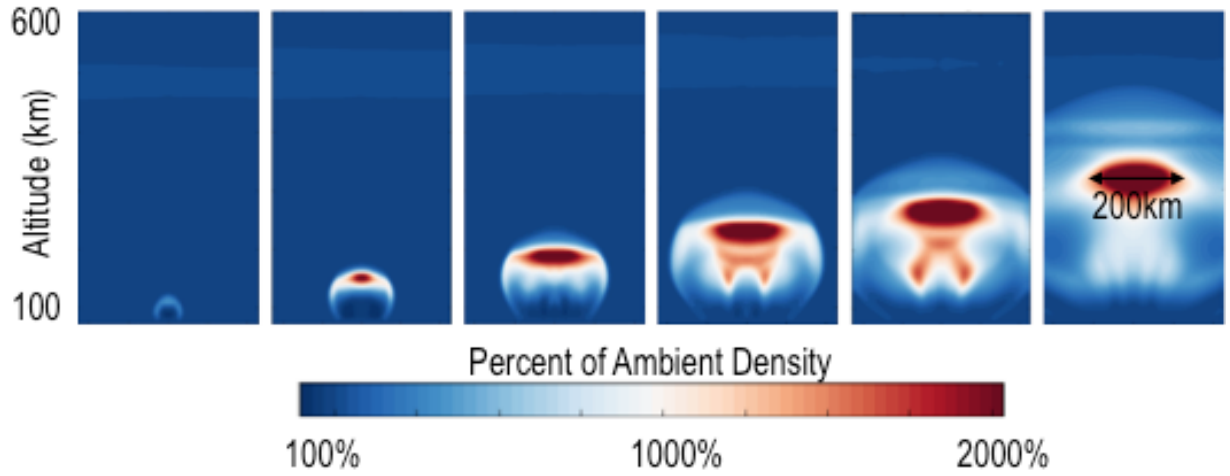

Figure 5: Phase 1 results indicate that a SpaDE system could achieve a 2000% increase in ambient density (ρ) at an altitude of 400 kilometers

The SpaDE air pulse will cause drag that de-orbits debris, calculated with the drag equation (1).

$$F_{Drag} = \frac{1}{2}\rho(\Delta v)^2 C_D A \quad (1)$$

In this equation, ρ is the density of the air pulse, Δv is the debris velocity relative to the pulse, C_D is the drag coefficient of the debris, and A is the reference area of the debris, estimated as its cross-sectional area. Of these factors, the only one SpaDE can influence is ρ, as the velocity is largely determined by orbital mechanics and the drag coefficient and reference area are properties of the debris. To cause orbital debris to re-enter the atmosphere, the air pulse needs to be at a higher density than the surrounding atmosphere when it reaches the debris.

In Phase 1 we modeled the pulse as a gravity wave, a wave generated in a fluid medium that is subject to the restoring force of gravity. We simulated explosions with varying energy and impulse as localized, instantaneous increases in pressure and temperature. We then added a vertical velocity component to the gravity wave to simulate an explosive direction that a SpaDE system could achieve with a range of technologies (e.g., shaped charges, air cannons). A detonation at an altitude of 80 km that produced a 40x increase in local temperature and a 3,000 km/hr vertical velocity resulted in a gravity wave propagating to suitable interception altitudes.

The air pulse is subject to gravity and therefore must be accelerated to reach the impact altitude. However, we discovered an initial wave that propagates ahead of the main wave. This wave acts likes a leading shock wave and reaches higher altitudes before gravity abates its effects.

Testing for this experiment included varying a wide range of temperature, velocity, and pressure starting conditions that were tested for this experiment. A negative starting temperature of the cell should be in theory have a higher ρ because of the ideal gas law. However, this was found to be not as effective as increasing the temperature. The reasons for this are not clear. It is clear that the initial velocity of the perturbation needs to be enough to ballistically lob the mass of air to the orbital altitude. This is the key factor to get the main portion of the perturbation to the debris interception altitude. Getting the velocity correct allows the air mass to stall at the apex and

provides a longer window of higher ρ for the debris. The stall effect happens because the air at the top starts to fall while the air at the bottom is still moving vertically up.

Figure 5 shows a run that tries to produce 2000% difference to ambient ρ. This is the approximate amount of ρ difference to bring down the majority of space debris within 1 orbit. This is not a requirement of the SpaDE system, but is a good study to show the necessary boundaries of the system. To bring down an object we need to reduce its velocity by 3%, about 228m/s for objects around 400km altitude going 7600m/s. Typical Cd is around 2.2 and traveling through the perturbation is about 30s. A/m is usually about .02. The ρ needed would be about 2e-9, which is about 2000 times bigger than the ambient ρ of about 1.0e-12.

A noted benefit to the SpaDE approach is the shape of the perturbation for this reaction. It is relatively thin disk shape, which is deal for trying to deal with the positional uncertainty of the debris as well as the timing of the start of the reaction.

The energy requirements for the perturbation in figure 2 are large. This perturbation requires the heating of a 6km x 6km x 4.8 km section of the atmosphere 50 times in temperature. With a mass density of roughly 1.81e-5 kg/m3 we are raising nearly 2M kg by 9800K, which is about 10.7e12J or equivalently 2.5 million kg of TNT. This is the limit case, and is not practical for deployment. However, in many situations it may not be necessary to de-orbit debris within a single orbit; changing the altitude of the orbit and lower the velocity will reduce predicted debris collisions with operational satellites, which we could achieve with other approaches, like using multiple smaller shots.

The one shot approach requires a significant amount of energy injected into the atmosphere, which may not be economical for eliminating debris. Bringing down debris in within a single orbit may not be the most optimal method of reducing the debris threat. Analyzing a lower energy level perturbation can be seen in figure 6. This series illustrates that there is a initial shock wave that travels ahead of the main pressure wave/mass transfer. Even when the pressure wave stops vertically propagating at a much lower altitude, the shock wave travels past 450km. This shock wave is travelling at approximately 1000m/s. Debris that moves through this region of the perturbation would have a vertical velocity gradient added to its velocity altering its trajectory. Adding a vertical velocity component to the debris trajectory will change its ephemeris lowering its perigee. The degree to which this will effect the debris is unknown at this time.

Another finding that figure 6 illustrates is the ballistic trajectory of the pressure wave of the perturbation. In this simulation, the pressure wave dissipates at about 180km. The reasons for this in part do to the initial velocity of the perturbation. Increasing the initial velocity increases this part of the perturbation allowing. Looking at the second high ρ wave that is seen clearly expanding at timestamp 120810 as a dark red blob from 130km to 160km in altitude, it can be seen dissipating over the next 120 seconds in the 5th and 6th frames. Comparing this to figure 5's pressure wave who's initial velocity was 10x the difference, the pressure wave reaches a higher altitude because the pressure does not have time to dissipate before reaching that altitude, but eventually this pressure wave will be dissipated and return to steady state.

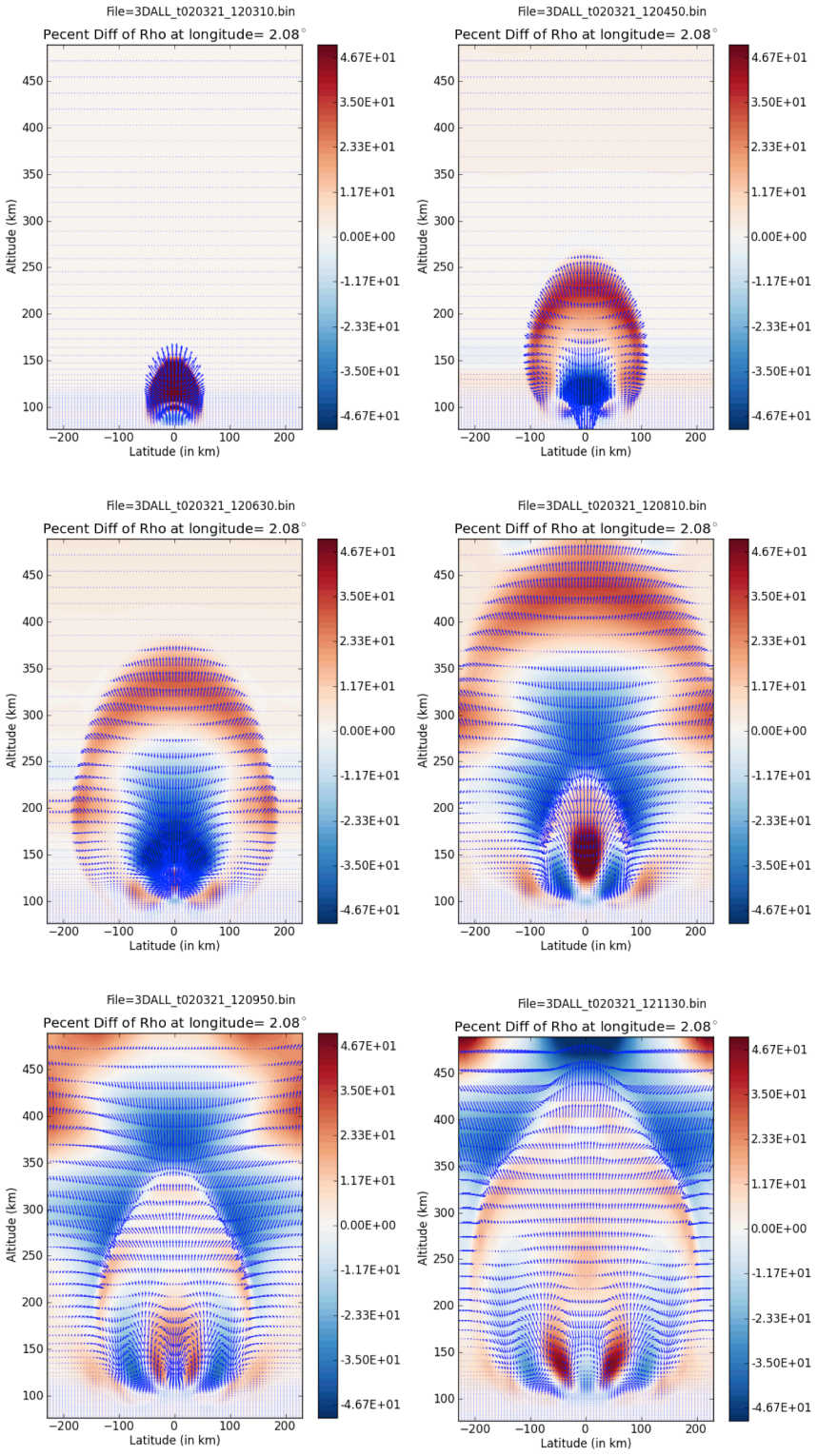

Figure 6: Low Energy Perturbation Series

5 Debris Behavior

We also analyzed debris behavior, in particular studying the effects of the perturbation on the debris using the results from the model data. We focused on the deltaV of the debris and the effective margin of error.

Correlating the force needed to produce a desired deltaV allows comparison of this method of debris reduction to other proposed methods. To calculate the drag effects on the debris, the standard drag equation is used. The GITM model calculated the ρ of the atmosphere, so we solved for the change in velocity in the drag equation:

$$\Delta v = \frac{1}{2}\rho v_d C_D D A/m \quad (1)$$

where ρ is the air density, v_d is the debris velocity, C_D is the drag coefficient, A is the cross-sectional area, D is the distance travelled and m is the mass of the debris.

The model calculates changes in the atmosphere at 10-second intervals. The time it takes a piece of debris to travel across the model boundaries is 25 seconds. To simplify the calculations, we used a single model slice to compute the drag on the debris. This approximation should be close enough to accurately model the debris behavior. For the diagram below, each point on the x-axis is a single time slice produced from the model. If a piece of debris with characteristics of C_D =1.6 and A/m=.01 were to fly through the model at 400km altitude, the velocity of the debris as it leaves the model will be shown on the y-axis.

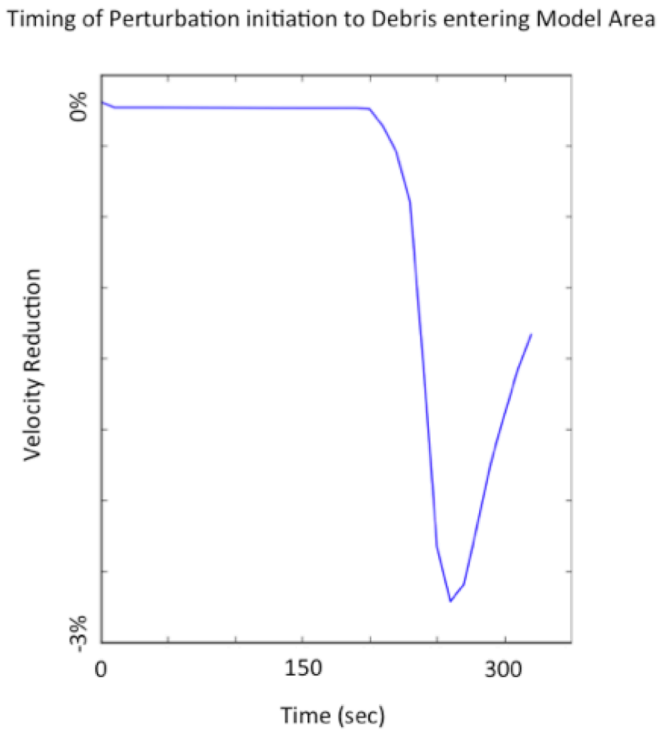

Figure 7: Temporal Perturbation Effects Diagram. X=0 represents the start of the simulation, so at about 254 seconds since the start of the perturbation we get the highest net velocity reduction on a piece of debris at 400km passing directly through the center of the perturbation.

Figure 7 shows the temporal perturbation effects on debris. Each point on the x-axis represents on time slice through the model and the y-axis measures the velocity reduction of a piece of debris the traverses across the model at 400km. The effectiveness of the SpaDE system peaks over a period of a minute, so timing is not a significant factor in the detonation of the perturbation. Space debris tracking accuracy can be off by

kilometers making the targeting difficult. SpaDE's effective area compensates for this targeting deficiency allowing for a 20km wide sweet spot that the debris can fly through and get over 90% of the maximum effectiveness.

Dr. Nicholas Johnson of the NASA Orbital Debris Program Office provided valuable insight to the structure and format of information that was used as inputs to his LEGEND and ORDEM modeling tools. He also was able to help improve understanding of the algorithms and processes of these modeling tools. This information will be used in great detail in any phase II work where we detail specific operational considerations of the SpaDE system. The information has also aided in sharpening our understanding of the specific challenges in planning and evaluating de-orbit planning and modeling of space debris.

6 Conclusion

In summary, SpaDE phase I has shown:

1. Perturbations at altitudes of approximately 80km can reach orbital debris at 600km
2. Expansion of the gas cloud propagates in the horizontal directions while keeping a compact vertical profile creating a disk
3. There is a leading "shock" wave the proceeds the pressure wave
4. Vertical velocity is required to move the mass to altitude
5. The sheer winds at 150km did not significantly affect the perturbation

SpaDE phase I showed that a compressed mass of atmosphere would stay coherent for altitudes up to 600km. The model shows that the gas dynamics allow for the perturbation to reach altitude with sufficient density to affect debris. Higher altitudes should be possible but were not tested in this study. Being able to heat and accelerate a large mass of atmosphere at 80km would take a large amount of energy.

The targeting aspect of space debris is reduced because of the large surface area that SpaDE is capable of producing. This surface area allows for lax timing in firing the perturbation and for compensating for the error of uncertainty in the debris position. These advantages are ideal for smaller debris (<10cm) targeting as well as fields of debris (i.e. multiple debris in close orbital proximity). SpaDE could be used for clearing a debris field after a satellite collision.

There is a leading shock wave that precedes the main propagation of mass. This shock wave could be used to steer debris around hazards or potentially changing the apogee and perigee of the debris. Changing the apogee and perigee of the debris could be used for hazard avoidance or it could be used to deorbit the debris sooner. Studies need to be done to determine the vertical component required to affect debris.

The initial vertical velocity of the perturbation follows ballistic trajectory. The GITM model is highly dependent on gravity and the effects of particles in the upper atmosphere that are affected by the gravitation force of the earth. SpaDE demonstrates that there is a relationship between the initial velocity and height of the perturbation.

The SpaDE concept appears to be a viable concept that could help eliminating debris in the lower parts of LEO. Although the energy requirements are high, they are not impractical. More work should be done to make the system more efficient and effective.

To advance SpaDE to TRL 3, we need to determine if the energy requirements can be reduced. Other modalities may help lower the energy requirements of the system and may provide additional performance benefits. Vortex rings, laminar flow, and simultaneous gravity waves appear to be promising modalities.

Another area for future study would be to estimate the effects of the shock wave that propagates ahead of the main pressure wave. This shock wave could be used to change the trajectory of the debris without changing the debris velocity. For objects in near circular orbits, this would have the effect of increasing their perigees and lowering their apogees. Lowering apogee will increase drag because the object is moving faster through denser air for that part of its orbit. However, such action could have side effects, the most important being that the new ephemeris could interfere with operational satellites. Another possible side effect of the SpaDE concept is that debris could skip off the perturbation. This could deorbit the debris faster, but it might create risks to operational satellites. And finally, we would like to determine the extent to which we could control the effects of the perturbation; for example, whether it would be possible to consistently place debris over the Pacific Ocean during their final descent into atmosphere.

7 References

Chamberlin, P. C., Woods, T. N., and Eparvier, F. G.: Flare Irradiance Spectral Model (FISM): Daily component algorithms and results, Space Weather, 5, S07005, doi:10.1029/2007SW000316, 2007.

Deng, Y., Richmond, A. D., Ridley, A. J., and Liu, H.-L.: Assessment of the non-hydrostatic effect on the upper atmosphere using a general circulation model (GCM), Geophys. Res. Lett., 35, L01 104, doi:10.1029/2007GL032182, 2008a.

Deng, Y., Ridley, A., and Wang, W.: Effect of the altitudinal variation of the gravita- tional acceleration on the thermosphere simulation, Geophys. Res. Lett., 113, A09302, doi: 10.1029/2007JA013081, 2008b.

Foster, J., Maurice, F.-P. S., and Abreu, V.: Joule heating at high latitudes, J. Geophys. Res., 88, 4885, 1983.

Fuller-Rowell, T. and Evans, D.: Height-integrated Pedersen and Hall conductivity patterns inferred from TIROS–NOAA satellite data, J. Geophys. Res., 92, 7606, 1987.

Hardy, D., Gussenhoven, M., Raistrick, R., and McNeil, W.: Statistical and fuctional representation of the pattern of auroral energy flux, number flux, and conductivity, J. Geophys. Res., 92, 12,275, 1987.

Heppner, J. and Maynard, N.: Empirical high-latitude electric field models, J. Geophys. Res., 92, 4467, 1987.

Hinteregger, H., Fukui, K., and Gibson, B.: Observational, reference and model data on solar EUV from measurements on AE-E, Geophys. Res. Lett., 8, 1147, 1981.

Newell, P. T., Sotirelis, T., and Wing, S.: Diffuse, monoenergetic, and broadband aurora: The global precipitation budget, J. Geophys. Res., 114, 09 207, doi:10.1029/2009JA014326, 2009.

Oehmke, R.: High Performance Dynamic Array Structures, Ph.D. thesis, University of Michigan, department of Electrical Engineering and Computer Science, 2004.

Oehmke, R. and Stout, Q.: Parallel adaptive blocks on the sphere, in: Proc. 11th SIAM Conf. Parallel Processing for Scientific Computing, SIAM, 2001.

Pawlowski, D. and Ridley, A.: Modeling the thermospheric response to solar flares, J. Geophys. Res., 113, A10 309, doi:10.1029/2008JA013182, 2008.

Pawlowski, D. and Ridley, A.: Quantifying the effect of thermospheric parameterization in a global model, J. Atmos. Sol-Terr. Phys., 71, 2017, doi:10.1016/j.jastp.2009.09.007, 2010.

1

Richards, P. G., Fennelly, J. A., and Torr, D. G.: EUVAC: A solar EUV flux model for

aeronomic calculations, J. Geophys. Res., 99, 8981, 1994.

Richmond, A.: Assimilative mapping of ionospheric electrodynamics, Adv. Space Res., 12, 59, 1992.

Richmond, A. and Kamide, Y.: Mapping Electrodynamic features of the high-latitude ionosphere from localized observations: Technique, J. Geophys. Res., 93, 5741–5759, 1988.

Ridley, A., Crowley, G., and Freitas, C.: An empirical model of the ionospheric electric potential, Geophys. Res. Lett., 27, 3675, 2000.

Ridley, A., Deng, Y., and To`th, G.: The global ionosphere-thermosphere model, J. Atmos. Sol-Terr. Phys., 68, 839, 2006.

Solomon, S., Hays, P., and Abreu, V.: The auroral 6300A˚emission: Observations and modeling, J. Geophys. Res., 93, 9867, 1988.

Tobiska, W. K.: Current status of solar EUV measurements and modeling, Adv. Space Res., 18, 3–10, doi:10.1016/0273-1177(95)00827-2, 1996.

Torr, D., Torr, M., Brinton, H., Brace, L., Spencer, N., Hedin, A., Hanson, W., Hoffman, J., Nier, A., Walker, J., and Rusch, D.: An experimental and theoretical study of the mean diurnal variation of O+, NO+, O2+, and N2+ ions in the mid-latitude F1 layer of the ionosphere, J. Geophys. Res., 84, 3360, 1979.

Weimer, D.: A flexible, IMF dependent model of high-latitude electric potential having ”space weather” applications, Geophys. Res. Lett., 23, 2549, doi:10.1029/2000JA000604, 1996.

Weimer, D. R.: Improved ionospheric electrodynamic models and application to calculating Joule heating rates, J. Geophys. Res., 110, 05 306, doi:10.1029/2004JA010884, 2005.

Woods, T. and Rottman, G.: Solar ultraviolet variability over time periods of aeronomic interest, Atmospheres in the Solar System: Comparative Aeronomy, Geophys. Monogr. Ser., 130, 221, 2002.

Woods, T. et al.: XUV Photometer System (XPS): Improved Solar Irradiance Algorithm Using CHIANTI Spectral Models, Solar Phys., 249, 235–267, 2008.

Woods, T. N., Eparvier, F. G., Bailey, S. M., Chamberlin, P. C., Lean, J., Rottman, G. J., Solomon, S. C., Tobiska, W. K., and Woodraska, D. L.: Solar EUV Experiment (SEE): Mission overview and first results, J. Geophys. Res., 110, 1312–+, doi:10.1029/2004JA010765, 2005.

Yig˘it, E. and Ridley, A. J.: Effects of high-latitude thermosphere heating at various scale sizes sim- ulated by a nonhydrostatic global thermosphere-ionosphere model, J. Atmos. Sol.-Terr. Phys., 73, 592, doi:10.1016/j.jastp.2010.12.003, 2011.

Yig˘it, E., Ridley, A., and Moldwin, M.: Importance of capturing heliospheric variability for stud- ies of thermospheric vertical winds, J. Geophys. Res., 117, doi:10.1029/2012JA017596,

Under Review, 2012.